



Design of continuous zoom collimating lens for Shack–Hartmann sensor

Hongzhuang Li¹ · Leqiang Yang¹ · Zhichen Wang¹ · Wenpan Wang¹ · Kainan Yao¹

Received: 14 January 2022 / Revised: 14 March 2022 / Accepted: 14 March 2022 / Published online: 9 June 2022
© The Korean Physical Society 2022

Abstract

A method to realize the change of spatial sampling rate of Shack–Hartmann wavefront sensor (SHWS) in telescope wavefront measurement using zoom collimating lens is proposed. First, the Gaussian optical formula is derived, and then, the optical system of the collimating lens is design and manufactured. After assembly and adjustment, the collimating lens is combined with Shack–Hartmann wavefront sensor, and the performance of the SHWS system is tested. The results show that the system achieves a changeable sampling rate from 19×19 to 12×12 . In the process of zooming, the wavefront error of the system is less than $\lambda/30$ RMS ($\lambda = 632.8$ nm), which achieve high performance of wavefront measurement, and meets the expected function requirements.

Keywords Shack–Hartmann Wavefront sensor · Wavefront measurement · Zoom collimating lens · Optical design

1 Introduction

Shack–Hartmann wavefront sensor is the key equipment for closed-loop wavefront error correction in the fields of adaptive optics, active optics and high-energy laser system. It is also an important wavefront measuring instrument in the fields of optical testing and ophthalmology diagnosis [1–4].

In adaptive and active optics system of large aperture telescope, there are different requirements for the performance of SHWS according to the target magnitude, skylight background and other observation conditions [5, 6]. When the observation conditions are good, and the magnitude of observation target is high, it is preferred to increase the spatial sampling rate to improve the sensitivity and measurement accuracy; when the observation conditions are poor, the observation target magnitude is low, and the effect of atmospheric disturbance is severe, it is preferred to reduce the sampling rate of the sensor to increase its detection ability, and increase the dynamic range of the sensor [7–9].

To enhance the adaptability under different observation conditions, SHWS with variable sampling rate are designed

in the adaptive optics system for many astronomical telescopes. For example, In the Very Large Telescope (VTL) of European Southern Observatory (ESO) [10], SHWS is equipped with two microlens arrays with different sampling rates (14×14 and 7×7), the 14×14 sampling rate is chosen to obtain higher detection accuracy when the observation conditions are good, and the 7×7 sampling rate is chosen to improve detection performance when the observation conditions are bad. In the adaptive optical system PALM-3000 of the 5.1 m Hale Telescope, four kinds of sampling rates, which includes 8×8 , 16×16 , 32×32 , and 64×64 for SHWS, are used under different observation conditions [11, 12]. In the new generation adaptive optics system of Keck Observatory, the natural guide star wavefront sensor (NGSWFS) also adopts SHWS with multiple sets of sampling rates [13].

In these systems, the variable sampling rate of SHWS is realized by switching multiple groups of microlens arrays, which will cause the waste of microlens arrays; In addition, fast switching cannot be achieved with this configuration.

Therefore, in 2003, Jungtae RHA and others used liquid crystal phase modulator to replace the traditional glass microlens array, which directly controlled the sub-aperture size of liquid crystal microlens array through electrical signal to change the sampling rate [14]. Baranec and Dekany proposed an SHWS based on electrically controlled segmented imaging mirror. The mirror is used as a wavefront

✉ Kainan Yao
longquanwanfa@163.com

¹ Changchun Institute of Optics, Fine Mechanics and Physics, Chinese Academy of Sciences, Changchun 130033, Jilin, China

segmentation device, and the segmented aperture and reflection angle of the mirror can be controlled by electrical signals; thus, it can realize the change of sampling rate [15].

The above two kinds of SHWS with variable sampling rate both use new electronically controlled segmented imaging devices to replace the traditional microlens array, but the new technology is still in the stage of research and development.

This paper proposed a method to realize the change of spatial sampling rate through continuous zoom collimating lens of SHWS. By changing the focal length of the collimating lens, the changes of the spatial sampling rate, dynamic range, sensitivity and other performance indexes of the sensor are realized.

Aiming at the design of continuous zoom collimation lens of SHWS, first, the Gaussian optical formula of two-component zoom collimating lens and the position change formula of telescope exit pupil during zoom are derived. And then, the optical system of the collimating lens is designed according to the index of a telescope wavefront measurement system. After manufacturing and alignment, the collimating lens is combined with the SHWS, and the performance of the system is tested. In the zoom process of the collimating lens, the sampling rate of the SHWS is changed from 19×19 to 12×12 , while the system wavefront error is ensured to less than $\lambda/30$ RMS ($\lambda = 632.8$ nm), which meets the expected functional and index requirements.

2 The relation between the focal length of collimating lens and indexes of SHWS

The configuration of wavefront measurement platform for telescope is shown in Fig. 1. The collimating lens is an important connecting component between the measured optical system and SHWS. Its function includes: (1) beam collimation. Ensures that the beam entered the sensor is collimated; (2) matching the spatial sampling rate, which is realized through the change of the exit pupil diameter; (3) matching the pupil position. The telescope pupil position is accurately imaged at the position of the microlens of SHWS through the collimating lens.

The exit pupil diameter is changed with different focal length of the collimating lens, so the sampling rate of the SHWS is changed. At the same time, the dynamic range and sensitivity of the sensor also change accordingly.

The dynamic range of SHWS describes the measurable maximum wavefront tilt at the entrance pupil of the telescope

$$\theta_{\max} = (\text{pitch}/f_p) \cdot (\text{EXP}/\text{ENP}), \quad (1)$$

pitch is the sub-aperture diameter of the lenslet array, f_p is the focal length of the lenslet, and ENP and EXP is the entrance pupil diameter and exit pupil diameter of the telescope, respectively.

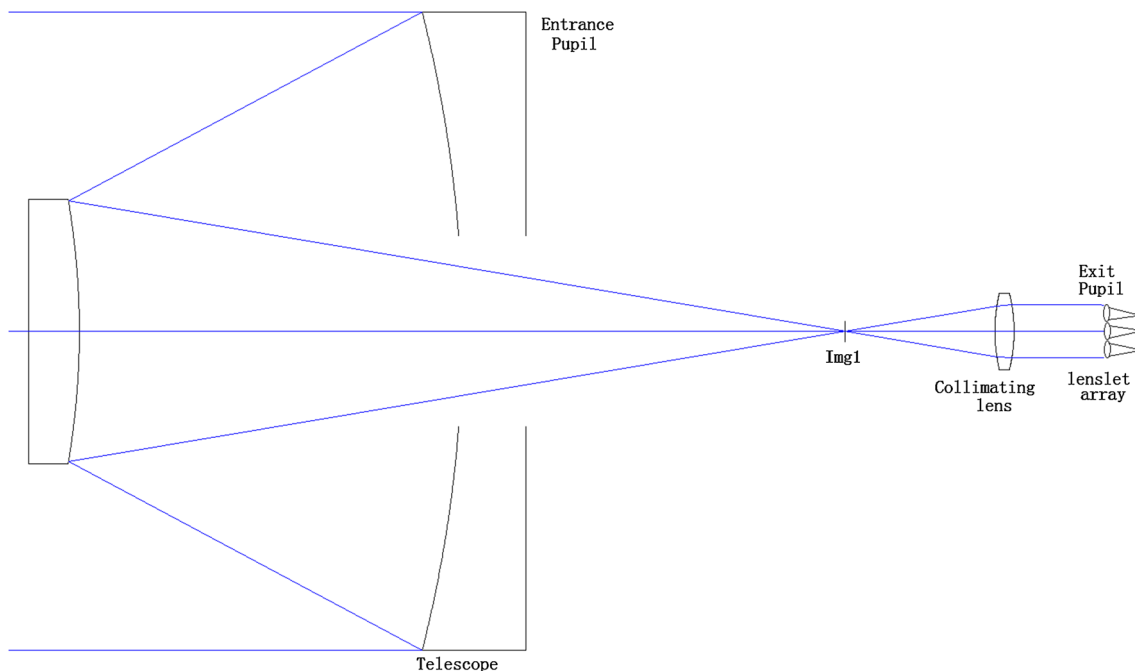


Fig. 1 Configuration of wavefront test for telescope

The sensitivity of SHWS represents the minimum measurable wavefront slope, which is limited by the calculation accuracy of spot centroid displacement

$$\theta_{\min} = (d_{\min}/f_p) \cdot (\text{EXP}/\text{ENP}), \tag{2}$$

d_{\min} is the minimum resolution distance of the spot offset of the lenslet array spot.

From the above formula, it can be seen that when the focal length of the collimating lens is increased, and the diameter of the telescope exit pupil *EXP* is increased, then the dynamic range of the sensor is increased and the sensitivity is reduced accordingly. On the contrary, when the focal length of the collimating lens is decreased, the diameter of the telescope exit pupil *EXP* and the measurement dynamic range of the sensor is reduced, but the sensitivity is improved accordingly.

3 Gaussian optics of zoom collimating lens

To ensure the simple structure, two-component mechanically compensated continuous zoom configuration is adopted [16, 17]. The configuration consists of two components: a zoom group and a compensation group. During the zoom process, the focal length of the lens changes linear with the movement

of the zoom group, and the image plane is remained stationary through the nonlinear movement of the compensation group.

The Gaussian optics configuration is shown in Fig. 2. In Fig. 2a, it defines f' as the focal length of the zoom group, f_2' as the focal length of the compensation group, and d as the distance between the zoom and compensation group. l_1 is the object distance of the zoom group, and the object of the collimating lens is the focus of the telescope (Img1); l_1' is the image distance of the zoom group.

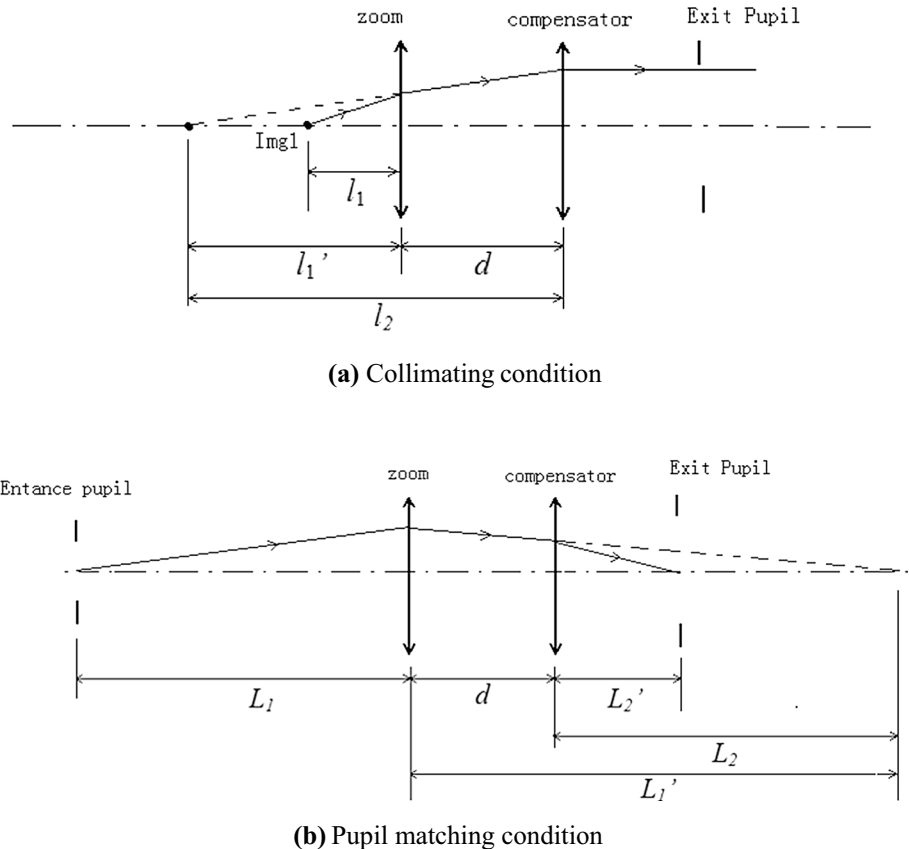
In Fig. 2b, L_1 is the distance between the telescope pupil and the zoom group, and L_1' is the pupil image distance after the zoom group. L_2 is the distance between the pupil image and the compensation group. L_2' is the pupil image distance after the compensation group. β_1 is the magnification of the zoom group, and the zoom ratio of the lens is defined as Γ .

In the zoom collimating lens, the zoom group moves x linearly, and the compensation group moves y accordingly to ensure that the beam is collimated. After moving, each amount is marked by “*”.

The zoom equations can be derived that

$$\begin{cases} l_1' = \frac{f_1' \cdot l_1}{f_1' + l_1} \\ l_1' + d = f_2' \end{cases} \tag{3}$$

Fig. 2 Gaussian optics of zoom collimating lens



$$\begin{cases} l_1^* = l_1 + x \\ l_1^{*'} = \frac{f_1' \cdot l_1^*}{f_1' + l_1^*} \\ d_* = f_2' - l_1^{*'} \\ y = d_* - d + x \end{cases} \quad (4)$$

$$\begin{cases} \beta_1 = \frac{l_1'}{l_1} \\ \beta_1^* = \frac{l_1^{*'}}{l_1^*} \\ \frac{\beta_1^*}{\beta_1} = \Gamma \end{cases} \quad (5)$$

From the formula (1), (2), and (3), the movement y of the compensation group corresponding to the movement x of the zoom group can be obtained.

In the process of zoom, the displacement of the telescope exit pupil position is defined as follows:

$$\begin{cases} L_1' = \frac{f_1' \cdot L_1}{f_1' + L_1} \\ L_2 = L_1' - d \\ L_2' = \frac{f_2' \cdot L_2}{f_2' + L_2} \end{cases} \quad (6)$$

$$\begin{cases} L_1^* = L_1 + x \\ L_1^{*'} = \frac{f_1' \cdot L_1^*}{f_1' + L_1^*} \\ L_2^* = L_1^{*'} - d^* \\ L_2^{*'} = \frac{f_2' \cdot L_2^*}{f_2' + L_2^*} \end{cases} \quad (7)$$

From the $L_1^{*'}, L_2^{*'}, d^*$ in the formula (4) and (5), the pupil position corresponding to the movement x of the zoom group can be calculated.

4 Design of zoom collimating lens

An SHWS testbed for a telescope with 1 m aperture diameter is designed and manufactured. According to the requirements, the sampling rate of the SHWS should be changed from 19×19 to 12×12 . As the pitch of the lenslet

is chosen to be 0.2 mm, the exit pupil diameter should be changed from 3.8 to 2.4 mm.

Then, the technical indexes of the collimating lens are defined as follows (see Table 1):

To balance the aberration and ensure the minimum spacing of each group, the focal length of the zoom group and the compensation group should be close to the focal length of the collimating lens at long focal position.

After repeated trial calculation using formula (1)–(5), the focal length of the zoom group and the compensation group is designed to be 24 mm and 22 mm, respectively. At the long focal position, the distance between the telescope focus and the zoom group is 2.5 mm, and the distance between the compensation group and the Exit pupil position is 4 mm. At the short focal position, the distance between the zoom group and the compensation group is 6.3 mm. Gaussian optical structure of the collimating lens is shown in Fig. 3.

The zoom compensation curves of the lens are shown in Fig. 4, which shows that the maximum movement of the zoom group and the compensation group is 7.2 mm and 6.1 mm, respectively. The movement curve is smooth, and can be realized through the cam mechanism easily.

Figure 5 shows the exit pupil position offset during zoom, the maximum offset is 1.29 mm, and the offset changes in the shape of a quadratic curve. Therefore, through repeated iteration of initial parameters, the pupil positions can be designed to be consistent at the long and short focal position, which is convenient for system application.

In the lens instruction design, both the zoom and compensation component are doublet, and the two components correct chromatic aberration separately. In the lens, the negative element adopts flint glass with high refractive index, and the positive power elements with low refractive index. The optical system layout is shown in Fig. 6.

The imaging quality of the optical system is shown in Figs. 7 and 8. It can be seen that the imaging quality of the systems is close to diffraction limiting, and the distortion at long focal position is less than 0.2%, and less than 0.5% at short focal position, respectively.

The collimating lens is designed in a large field of view ($\pm 18^\circ$); however, due to the accurate tracking system with

Table 1 Technical indexes of collimating lens

Index	Parameter
Object space numerical aperture	0.095
Focal length	20 mm–12.6 mm
Zoom ratio	1.58 \times
Exit pupil diameter	3.8–2.4 mm
Field of view (FOV)	5.49°–8.7°
Corresponding telescope FOV	$\pm 18''$
Spectral range	500–700 nm

Fig. 3 Gaussian optical structure of the collimating lens

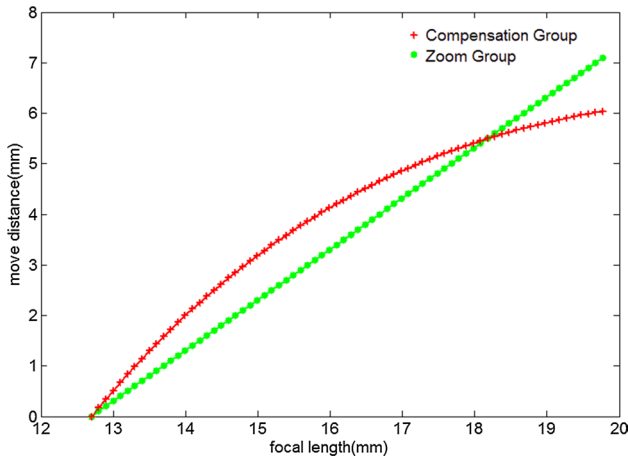
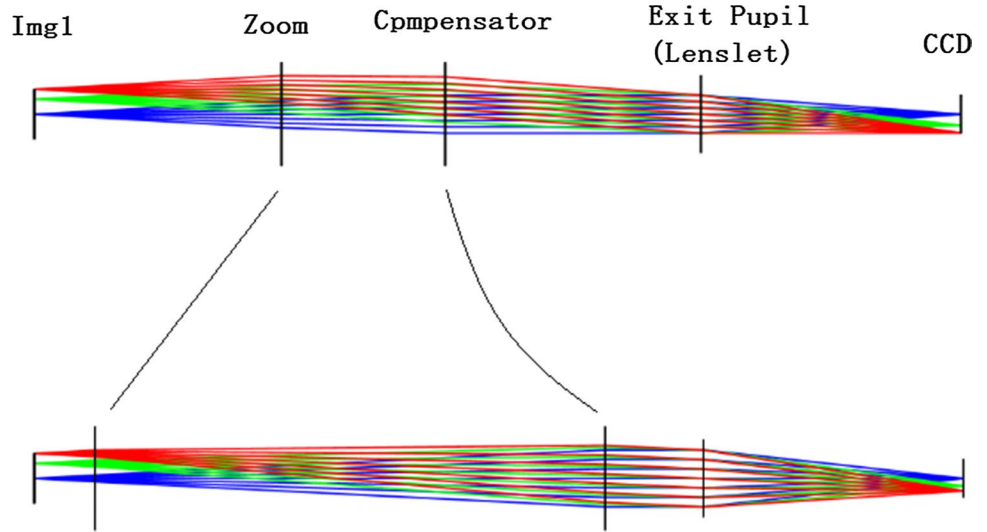


Fig. 4 Zoom compensation curve

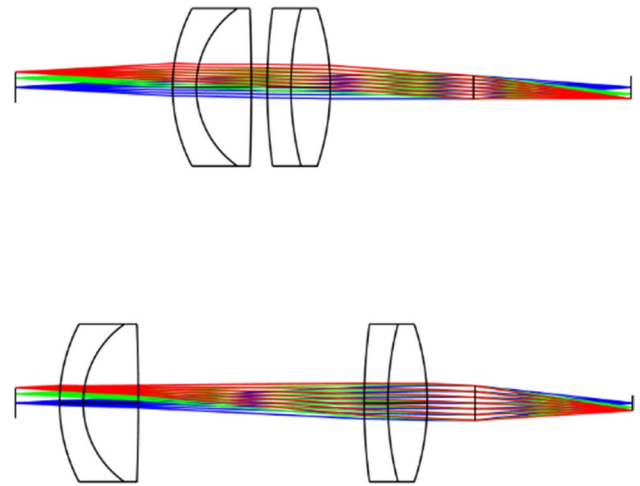


Fig. 6 Optical system layout of the zoom collimating lens

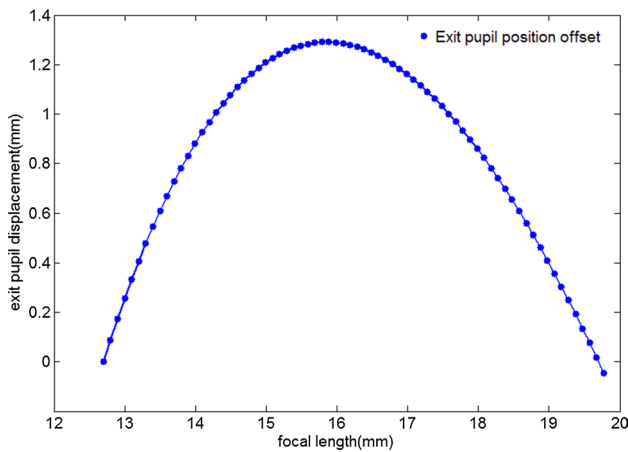


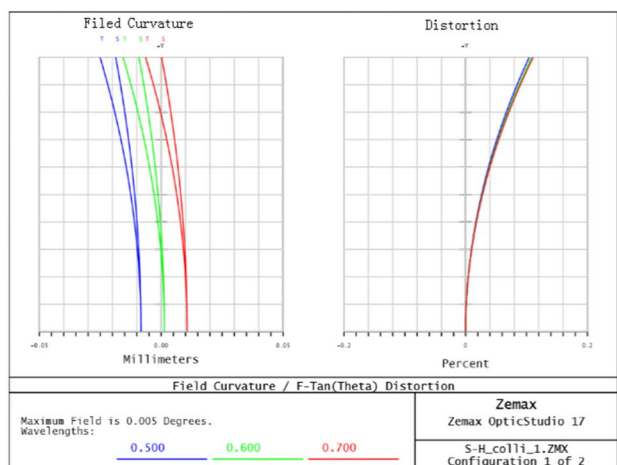
Fig. 5 Exit pupil position offset curve

fast steering mirror in the adaptive optics system, the field of view of the wavefront measurement can be stabilized in a very small range, generally less than $\pm 2''$.

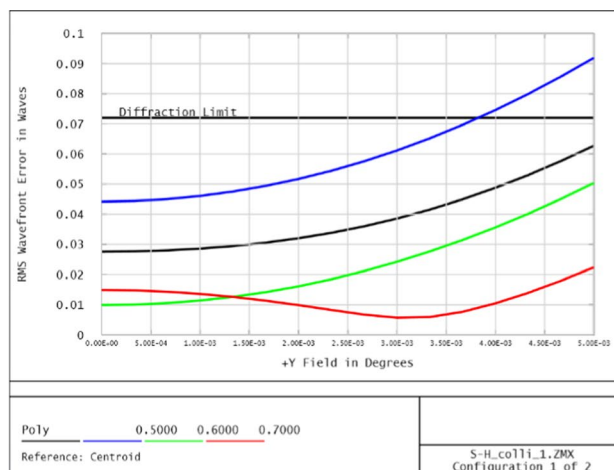
The spot diagram within the field of view of $\pm 2''$ is shown in Fig. 9. It can be seen that the panchromatic image spots are within the optical diffraction limit, which will not have a significant impact on the wavefront measurement.

5 Experimental setup and results

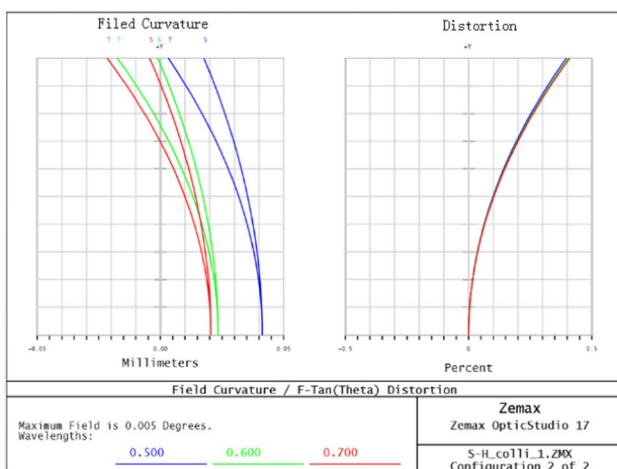
Through structural design, the zoom and compensation group are installed in the designed cam slot, respectively, and the two groups move along the optical axis on the guide rail driven by the motor, according to the zoom curve in the cam slot, as shown in Fig. 10.



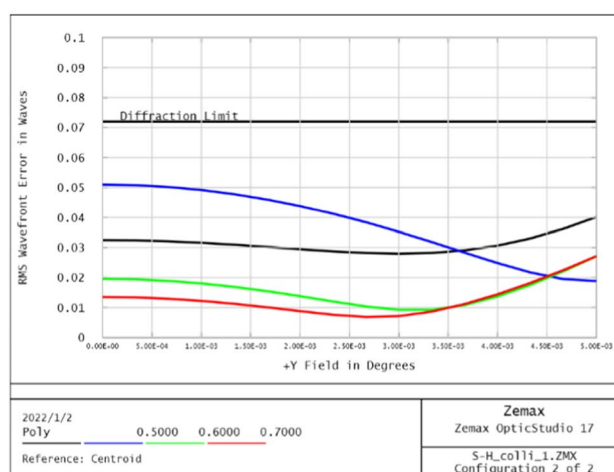
(a) f20mm



(a) f20mm



(b) f12.6mm



(b) f12.6mm

Fig. 7 Aberration curves at long and short focal positions

To test the performance of the system, the collimating lens and SHWS are combined. The SHWS is first calibrated with ideal beam from Zygo interferometer, which can get rid of the systematic error of the sensor, as shown in Fig. 11.

Then, the SHWS and the collimating lens are combined and aligned, as shown in Fig. 12, and a fiber source is used to simulate the telescope focus. The divergent beam from the fiber is collimated by the collimating lens. And during the zooming of the collimating lens, the diameter of the collimated beam changes continuously, and then, the sample rate of the SHWS changes continuously.

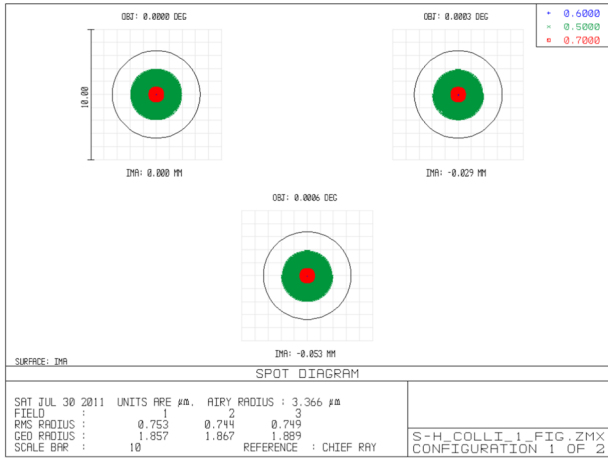
The tested wavefront error is reconstructed using 35 terms Zernike aberrations.

Since the exit pupil position will have a maximum offset of 1.29 mm during zoom, the SHWS is installed on an adjustment table for pupil position matching.

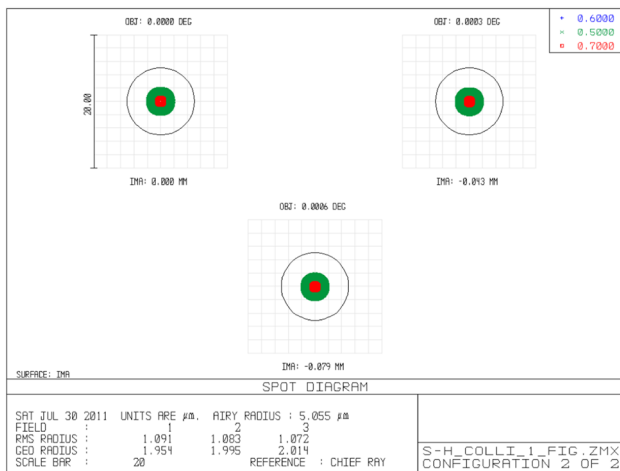
Fig. 8 Wavefront error at long and short focal positions

The wavefront test result is shown in Fig. 13; at the long focal position of the collimating lens, the sampling rate reaches 19×19 , and the measured wavefront error RMS is 0.027λ ($\lambda = 632.8$ nm). At the short focal position, the sampling rate reaches about 12×12 , and the measured wavefront error RMS is 0.018λ .

The wavefront error changes during the process of zooming, as shown in Fig. 14. It can be seen that, due to the increase of the optical aperture, the wavefront error of the system increases along with the sampling rate of the SHWS, but they are less than $\lambda/30$ RMS in the whole process of zooming, which is under the diffraction limiting, and the defocus and other aberrations of the wavefront are negligible.



(a) f20mm



(b) f12.6mm

Fig. 9 Spot diagram at long and short focal positions in $\pm 2''$ FOV



Fig. 10 Zoom collimating lens



Fig. 11 SHWS calibration using Zygo

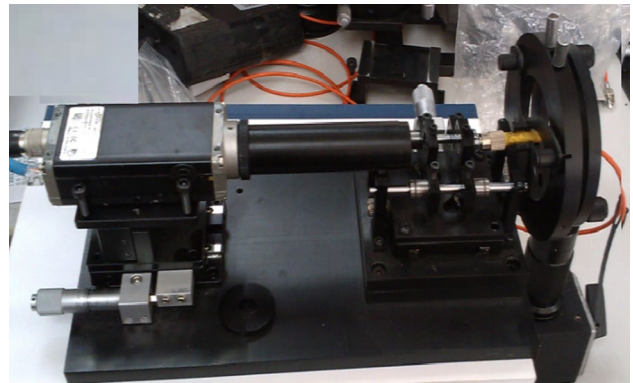


Fig. 12 Combined system of collimating lens and SHWS

6 Conclusion

A method to realize the change of spatial sampling rate of SHWS in telescope wavefront measurement using a zoom collimating lens is proposed. A zoom collimating lens is designed and manufactured based on the Gaussian optics. Then, the experimental testbed is assembled with a SHWS. The performance of the system is tested. The test results show that the system realizes the sampling rate change from 19×19 to 12×12 , and the wavefront error in the zoom process is less than $\lambda/30$ RMS. The results show that the collimating lens achieves the expected collimation and zoom function, and the performance meets the application requirements in engineering.

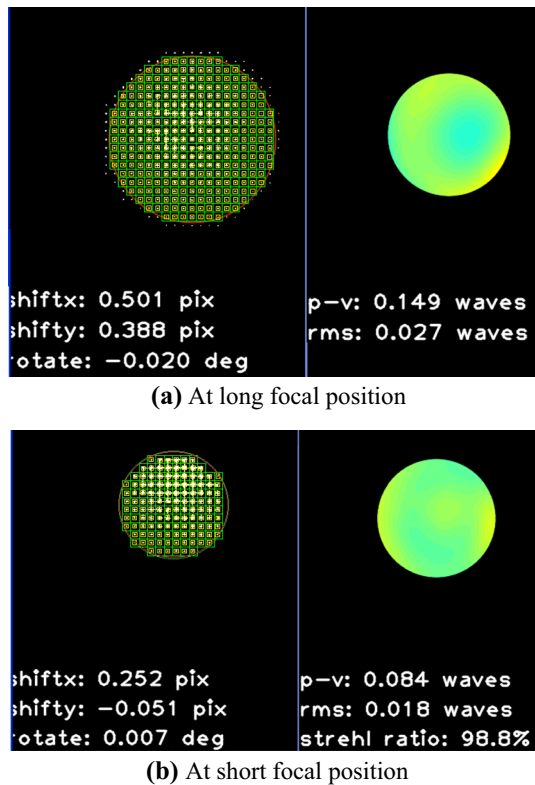


Fig. 13 Wavefront measurement results from SHWS

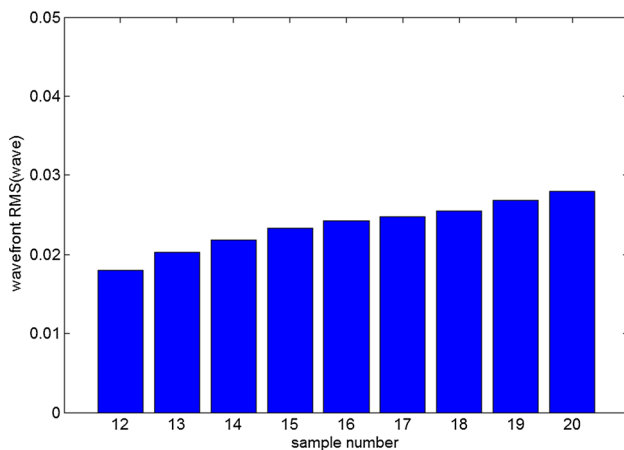


Fig. 14 Wavefront RMS from SHWS with different sampling rate

Funding Department of Science and Technology of Jilin Province(20210201020GX).

References

1. B.C. Platt, R.V. Shack, History and principles of Shack-Hartmann wavefront sensing. *J. Refract. Surg.* **17**(5), S573 (2001)
2. D.R. Neal, J. Copland, D.A. Neal, Shack-Hartmann wavefront sensor precision and accuracy. *Proc. SPIE* **4779**, 148–160 (2002)
3. J. Primot, Theoretical description of Shack-Hartmann wave-front sensor. *Opt. Commun.* **222**(1), 81–92 (2003)
4. R.R. Rammage, D.R. Neal, R.J. Copland, Application of Shack-Hartmann wavefront sensing technology to transmissive optic metrology. *Proc. SPIE - Int. Soc. for Opt. Eng.* **4779**, 161–172 (2002)
5. J.E. Greivenkamp, D.G. Smith, R.O. Gappinger, G.A. Williby, Aspheric metrology with a Shack-Hartmann wavefront sensor. *Proc. SPIE* **4419**, 1–4 (2001)
6. D.R. Neal, D.M. Topa, J. Copland, The effect of lenslet resolution on the accuracy of ocular wavefront measurements. *Proc. SPIE* **4245**, *Ophthalmic Technol.* **XI**, (2001)
7. R.G. Lane, M. Tallon, Wavefront reconstruction using a Shack-Hartmann sensor. *Appl. Opt.* **31**(32), 6902–6908 (1992)
8. L. Seifert, J. Liesener, H. Tiziani, The adaptive Shack-Hartmann sensor. *Opt. Commun.* **216**, 313–319 (2003)
9. J. Pfund, N. Lindlein, J. Schwider, Dynamic range expansion of a Shack-Hartmann sensor by use of a modified unwrapping algorithm. *Opt. Lett.* **23**, 995–997 (1998)
10. P. Feautrier, P.Y. Kern, R.J. Dorn et al., Naos visible wavefront sensor. *Proc. SPIE* **4007**, 396–407 (2000)
11. R. Dekany, A. Bouchez, M. Britton et al., PALM-3000: visible light AO on the 5.1-meter Telescope. *Int. Soc. Opt. Photonics* **6272**, 62720G (2006)
12. C. Baranec, N. Hubin, C.E. Max et al., High-order wavefront sensing system for PALM-3000. *Proc. SPIE - Int. Soc. Opt. Eng.* **7015**, 70155M (2008)
13. P. Wizinowich Adkins, S. Dekany, et al. W. M. Keck Observatory's next-generation adaptive optics facility. *Proc. SPIE* **7736**, *Adapt. Opt. Syst.* **II**, 77360K (2010)
14. J. Rha, D.G. Voelz, M.K. Giles, Reconfigurable Shack-Hartmann wavefront sensor. *Opt. Eng.* **43**(1), 251–256 (2004)
15. C. Baranec, R. Dekany, Study of a MEMS-based Shack-Hartmann wavefront sensor with adjustable pupil sampling for astronomical adaptive optics. *Appl. Opt.* **47**(28), 5155–5162 (2008)
16. T. ChunKan, Varifocal differential equation theory of zoom lens. *SPIE* **2539**, 168–179 (2001)
17. L. Yang, K. Yao, J. Wang et al., Performance analysis of 349-element adaptive optics unit for a coherent free space optical communication system. *Sci. Rep.* **9**, 13150 (2019)

Publisher's Note Springer Nature remains neutral with regard to jurisdictional claims in published maps and institutional affiliations.